analytical chemistry

pubs.acs.org/ac Article

SERS Sensors Based on Aptamer-Gated Mesoporous Silica Nanoparticles for Quantitative Detection of *Staphylococcus aureus* with Signal Molecular Release

Afang Zhu, Tianhui Jiao, Shujat Ali, Yi Xu, Qin Ouyang,* and Quansheng Chen*

Cite This: *Anal. Chem.* 2021, 93, 9788−9796 Read Online

ACCESS | Metrics & More | Article Recommendations | Supporting Information

ABSTRACT: This work describes a simple and novel biosensor for the quantitative determination of *Staphylococcus aureus* (*S. aureus*) based on target-induced release of signal molecules from aptamer-gated aminated mesoporous silica nanoparticles (MSNs) coupled with surface-enhanced Raman scattering (SERS) technology. MSNs were synthesized and then modified with amino groups by (3-aminopropyl) triethoxysilane to make them positively charged. Next, signal molecules (4-aminothiophenol, 4-ATP) were loaded into the pores of MSNs. Then, negatively charged aptamers of *S. aureus* were assembled on the surface of MSNs through electrostatic interactions. Upon the addition of *S. aureus*, the assembled aptamers were specifically bound to the bacteria. Consequently, the "gates" were opened, resulting in the release of 4-ATP from the pores of MSNs. The released molecules were measured by a Raman spectrometer, and the intensity of 4-ATP at 1071 cm^{-1} was linearly related to the *S. aureus* concentration. A silver nanoflower silica core−shell structure (Ag NFs@SiO_2) was prepared and it served as a SERS substrate. Under optimized experimental conditions, a good linear relationship (y = 2107.93 + 1536.30x, R^2 = 0.9956) in the range from 4.7 × 10 to 4.7 × 10^8 cfu/mL was observed with a limit of detection of 17 cfu/mL. The method was successfully applied for the analysis of *S. aureus* in fish samples and the recovery rate was 91.3−109%.

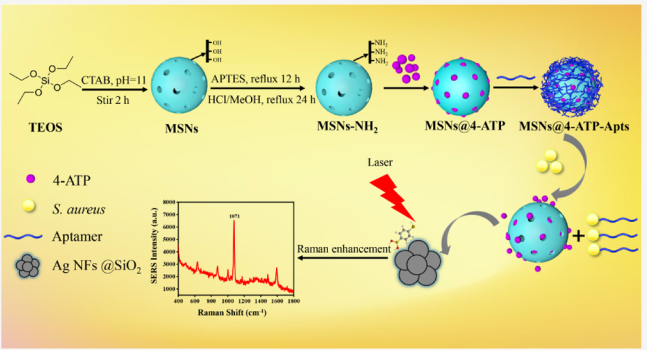

1. INTRODUCTION

Staphylococcus aureus (*S. aureus*) is a widely spread food-borne pathogen and can be found in the air, water, dust, and excretion of humans and other animals.[1] *S. aureus* pollutes food, seriously affects food safety, and is a threat to consumers' health. Currently, food poisoning caused by *S. aureus* is one of the major food safety issues that pose substantial health hazards.[2] Raw fish and its products are highly susceptible to microbial contaminations during processing, transportation, and sales.[3] *S. aureus* contaminates meat and its products seriously. Therefore, sensitive detection of *S. aureus* in meat is of crucial importance for food safety and human health.

So far, several methods such as plate culture method,[4] enzyme-linked immunosorbent assay,[5] molecular biological detection, for example, polymerase chain reaction,[6] have been focused on the determination of foodborne pathogens in different matrices. These methods not only require expensive instruments and highly skilled workers but also involve intricate sample pretreatments and are time-consuming,[7−9] hence limiting their application in food safety and security. Consequently, it is particularly important to establish a simple, sensitive, and specific method for the quantitative detection of *S. aureus*.

Surface-enhanced Raman scattering (SERS) is a very effective fingerprint recognition technique that provides comprehensive information about the vibrational characteristics of a molecule and reflects the actual molecular fingerprint.[10−12] SERS technique can detect ultra-trace levels of analytes up to single molecular level[13] and has attracted much attention in biomedicine,[14] materials science,[15] food safety,[16,17] engineering, and environmental monitoring.[18] The high sensitivity of SERS is primarily due to the massive electromagnetic (EM) enhancement generated on the surface of a nanostructured noble metal associated with localized surface plasmon resonance (SPR).[19,20] The enhancement strongly depends on the SERS substrate, test analyte, morphology and size of the nanomaterial, type of metal, and excitation wavelength.[21,22] Gold (Au) and silver (Ag) are the most popular active SERS substrates because they are reasonably easy and cheap to fabricate on a commercial level

Received: March 24, 2021
Accepted: June 29, 2021
Published: July 8, 2021

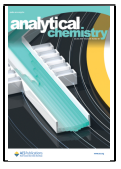

https://doi.org/10.1021/acs.analchem.1c01280
Anal. Chem. 2021, 93, 9788−9796

combined with the visible and NIR wavelengths of the SPRs.[23] Silver has a stronger enhancement effect than gold and is widely used to make Raman-active substrates. However, there are still some obvious defects, such as easy aggregation, active chemical properties, and ease of chemical reaction with external substances, which lead to SERS deterioration and seriously affect SERS performance of the substrate.[24] Recently, core−shell structures have been used in the preparation of SERS substrates. The thin shell composed of inert materials successfully prevents the noble metal-core from contacting the outside environment and improves the relative performance of the nanomaterial. As an inert material, silica is an ideal shell material because it has no absorbance in the visible light band and has certain hydrophilicity.[25] For instance, Li et al. have applied spherical Au@SiO_2 core−shell nanoparticles as a sensitive SERS substrate and realized the rapid quantitative analysis of Hg^{2+} residue in dairy products.[26] Mesoporous silica nanoparticles (MSNs) have been extensively studied in various fields due to their high surface area, uniform and adjustable pore diameter and particle size, large pore volume, easy surface functionalization, and exceptional biocompatibility.[27]

Compared with other support materials, MSNs have unique advantages in structure and properties such as the ordered and porous structure of mesoporous silica, which gives it a large specific surface area and pore volume, which enables it to load more molecules and to control the molecular release. Similarly, the particle size of MSNs can be controlled between 50 and 300 nm; the outer surface and inner pore surface of MSNs are easy to be functionalized, and the volume and release behavior of cargos can be better controlled by surface functionalization. Furthermore, studies have proved the exceptional biocompatibility and low cytotoxicity of MSNs.[28,29] The large specific surface area of MSNs provides sufficient space sites and makes it possible to load large numbers of cargos by different gates and diverse design strategies.[30] MSNs are promising candidates for loading a wide range of substances, which has attracted significant attention in developing "turn-off−on" sensing platforms. Tang et al. have designed a novel fluorescence immunoassay method based on target-induced cargo release from protein-gated carbohydrate-functionalized magnetic MSNs and successfully realized the detection of aflatoxin.[28] Zhang et al. have established a new homogeneous immunoassay strategy based on target-responsive cargo release from a polystyrene microsphere-gated mesoporous silica nanocontainer, which was applied to the quantitative detection of brevetoxin B.[31] An aptamer is a nucleotide sequence obtained from an ssDNA or RNA library containing 10^{13} to 10^{15} random sequences by Systematic Evolution of Ligands by Exponential Enrichment technology.[32] The aptamers can specifically capture the target bacteria and can be applied to achieve the specific recognition of bacteria.

Hence, a novel and sensitive approach was assembled for the detection of *S. aureus* using SERS technology based on the targeted responsive release of the signal molecules (4-aminothiophenol, 4-ATP) from aptamer-gated MSNs. First, MSNs were synthesized by the sol−gel method, and the amino group was modified by (3-aminopropyl) triethoxysilane (APTES) on their surface to make them positively charged. Second, 4-ATP was successfully loaded in the pores of the MSNs. Then, the aminated MSNs were coated by negatively charged aptamers via electrostatic interaction. The aptamers served as "gates" to prevent the release of the signal molecule. In the presence of *S. aureus*, aptamers were bound to the bacteria, resulting in opening of the gates and then induced the release of 4-ATP from the pores. The released signal molecules were monitored by a Raman spectrometer, and the signal was positively correlated with the concentration of the bacterial solution. *S. aureus* concentration was calculated by the SERS intensity of 4-ATP at 1071 cm^{-1}.

2. MATERIALS AND METHODS

2.1. Reagents and Materials. Analytical-grade chemicals and solvents were used in this experiment (without further purification). L-Ascorbic acid (AA, ≥99.0%) and APTES were bought from Sigma-Aldrich (USA). Tetraethyl orthosilicate (TEOS), cetyltrimethylammonium bromide (CTAB), aqueous ammonia solution ($NH_3{\cdot}H_2O$), trisodium citrate dihydrate ($C_6H_5Na_3O_7{\cdot}2H_2O$), sodium hydroxide (NaOH), silver nitrate ($AgNO_3$, ≥99.8%), methanol, absolute ethanol (C_2H_5OH), hydrochloric acid (HCl, 36%), and polyvinylpyrrolidone (PVP, K30) were purchased from Sinopharm Chemical Reagent Co., Ltd. (Shanghai, China). *S. aureus* (ATCC 29213), *Escherichia coli* (ATCC 12435), *Salmonella* (ATCC 14028), and *Listeria monocytogenes* (ATCC 19115) strains were acquired from the American Type Culture Collection (ATCC). *Bacillus subtilis* (BNCC 251376) and *Pseudomonas* (BNCC 125486) strains were obtained from BeNa Culture Collection (BNCC). *Vibrio parahaemolyticus* (CICC 10392) was purchased from the China Center of Industrial Culture Collection (CICC). The aptamer sequence of *S. aureus* (5′-GCAATGGTACGGTACTTCCTCGG-CACGTTCTCAGTAGCGCTCGCTGGTCATCCCA-CAGCTACGTCAAAAGTGCACGCTACTTTGCTAA-3′)[33] was synthesized by Shanghai Biotechnology Co., Ltd. Fresh fish was purchased from a local RT-Mart supermarket in a sealed plastic pack and stored in a refrigerator at 4 °C before the experiment. All solutions were prepared in Milli-Q water (resistivity >18 MΩ cm) from a Millipore water purification system.

2.2. Instrumentations. TEM images were acquired with a transmission electron microscope (JEM-2100HR; JEOL Ltd., Japan). Infrared spectra were collected by a Fourier-transform infrared (FT-IR) spectrophotometer (Thermo Electron Co., U.S.A.). Raman spectra were attained by an SPLD-RAMAN-785-Q spectrometer (Hangzhou SPL Photonics Co Ltd., China) equipped with a 785 nm laser excitation. Ultraviolet−visible (UV−vis) absorption spectra were recorded by an 8454 UV−vis spectrophotometer (Agilent Technologies Inc., USA). X-ray diffraction (XRD) pattern analysis was carried out using a D8-ADVANCE instrument (Bruker AXS Ltd., Germany). The morphology and size of the synthesized nanoparticles were observed by a field-emission scanning electron microscope (JSM-7800F; FE-SEM, JEOL Ltd., Japan). Energy-dispersive spectroscopy (EDS) spectra of the nanoparticles were recorded by an EDS instrument (S-3400N; Hitachi Ltd., Japan). The ζ potential was measured using a Nano-ZS Zetasizer ZEN3600 (Malvern Instruments Ltd., U.K.).

2.3. Preparation of the *S. aureus* Suspension. The purchased lyophilized *S. aureus* (ATCC 29213) powder was initially dissolved in sterile saline and then activated and cultured in Lysogeny Broth medium under aerobic conditions at 37 °C for 12 h on a shaker. Then, 20 mL of *S. aureus* solution was taken in a 50 mL sterile tube. For analysis, the bacterial solution was centrifuged at 6000 rpm for 10 min and the supernatant was removed and re-dispersed in 20 mL of sterile saline. Finally, the bacterial suspension was serially

https://doi.org/10.1021/acs.analchem.1c01280
Anal. Chem. 2021, 93, 9788−9796

Scheme 1. Schematic Illustration of *S. aureus* Detection Based on the Target-Responsive Release of 4-ATP Molecules from Aptamer-Gated MSNs

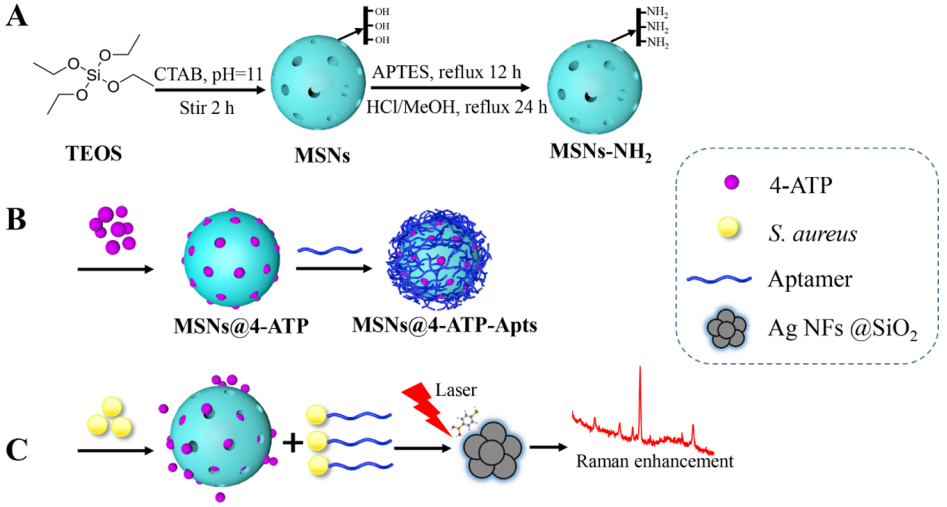

diluted by a 10-fold concentration gradient. At the same time, the traditional plate counting method was used to determine the total number of colonies in each concentration gradient, and three parallel experiments were carried out.

2.4. Preparation of a Silver Nanoflower Silica Core–Shell Structure (Ag NFs@SiO_2). *2.4.1. Synthesis of Silver Nanoflowers.* Ag seeds were synthesized by reducing Ag ions with sodium citrate following a previous method.[34] Briefly, 5 mM $AgNO_3$ solution (100 mL) was heated to boiling under constant stirring. 10 mL of 0.02 g/mL sodium citrate solution was added dropwise to the boiling solution and magnetic stirring was performed for 1.5 h to ensure that the Ag ions in the reaction mixture were completely reduced. After completion of the reaction, the reaction mixture was cooled to room temperature (RT) and a yellowish solution of Ag seeds was obtained. Subsequently, silver nanoflowers (Ag NFs) were synthesized as described previously with minor adjustments.[35] First, 15 mL of Ag seed solution was added to 20 mL (10 mM) of ascorbic acid solution under continuous stirring. Second, 10 mL of $AgNO_3$ solution (100 mM) was rapidly added into the above solution through a micropipette at RT. After a few seconds, the color of the mixture changed from yellowish to black. The obtained mixture was kept for 2 h and then the supernatant was removed. Finally, the precipitates after centrifugation were repeatedly washed with deionized water and absolute ethanol and dispersed in 45 mL ethanol/water solution (ethanol/water = 3:1, v/v).

2.4.2. Preparation of the Ag NFs@SiO_2 Substrate. Modification of the prepared Ag NFs was achieved by adding 0.4 g of PVP and constantly stirring for 1 h at RT. The modified Ag NFs were subsequently centrifuged at 6500 rpm for 10 min and suspended in 100 mL of the ethanol/water (1:1) solution. Then, 5 mL of $NH_3{\cdot}H_2O$ (25%) and 150 μL of TEOS (99%) were injected into the reaction mixture. The mixture was continuously stirred for 24 h at RT to ensure a uniform coating. Finally, the solution was centrifuged at 8500 rpm for 10 min and washed alternately with deionized water and ethanol. The obtained SiO_2-capped Ag NFs were stored at 4 °C for further use.

2.5. Preparation of Aminated MSNs. MSNs were prepared according to a reported procedure.[36] First, 1 g of CTAB was dissolved in 480 mL of deionized water. Next, 3.5 mL of NaOH aqueous solution (2 M) was slowly added to the as-prepared CTAB solution at an adjusted temperature (80 °C) and the mixture was stirred to react for 20 min. Then, 5 mL of TEOS was added dropwise to the reaction mixture under vigorous stirring and the mixture was reacted for 2 h, which resulted in a white precipitate. After cooling, the filtered solid crude product was washed with water and methanol and dried to obtain MSNs without removing the template. The aminated MSNs were prepared according to the literature with minor modifications.[37] The synthesized MSNs without removing the template were initially dispersed in 50 mL of ethanol, 0.7 mL of APTES was added, and the mixture was refluxed under a nitrogen environment at 80 °C for 12 h. The MSNs–NH_2 were separated by centrifugation, washed three times with ethanol, and dried. Afterward, the synthesized amino-modified MSNs were dispersed in 160 mL of methanol solution containing 9 mL of HCl (37.4%), and the reaction was refluxed for 24 h to remove the surfactant CTAB. After completion of the reaction, the product was filtered, washed with water and methanol, and dried under vacuum to obtain aminated MSNs.

2.6. Preparation of Signal Molecule-Loaded MSNs Capped with Aptamers. The loading of signal molecules into the pores of aminated MSNs was carried out according to a previously reported method.[37] Briefly, 5 mg of the amine-functionalized MSNs was initially dispersed in 500 μL of PBS (pH 7.5) buffer solution containing 2.5 M signal molecules, and the resulting mixture was then gently shaken on a shaker for 12 h at RT. During this process, 4-ATP molecules were diffused into the pores of the aminated MSNs and then 500 μL of wrapping aptamers (10 μM) was added into the resulting suspension. The mixture was gently stirred for 4 h at 25 °C. Owing to the interaction between positively charged MSNs and negatively charged aptamers, the wrapping aptamers were attached to the surface of the APTES-functionalized MSNs and enclosed the signal molecules inside. Then, the aptamer-wrapped MSNs were centrifuged and washed with distilled water to remove the excess 4-ATP molecules and aptamers until a low SERS signal and low UV–vis absorption spectrum of aptamers were obtained. Finally, the aptamer-capped MSNs loaded with signal molecules were re-dispersed in 500 μL of PBS buffer solution (pH 7.5) for further use.

https://doi.org/10.1021/acs.analchem.1c01280
Anal. Chem. 2021, 93, 9788–9796

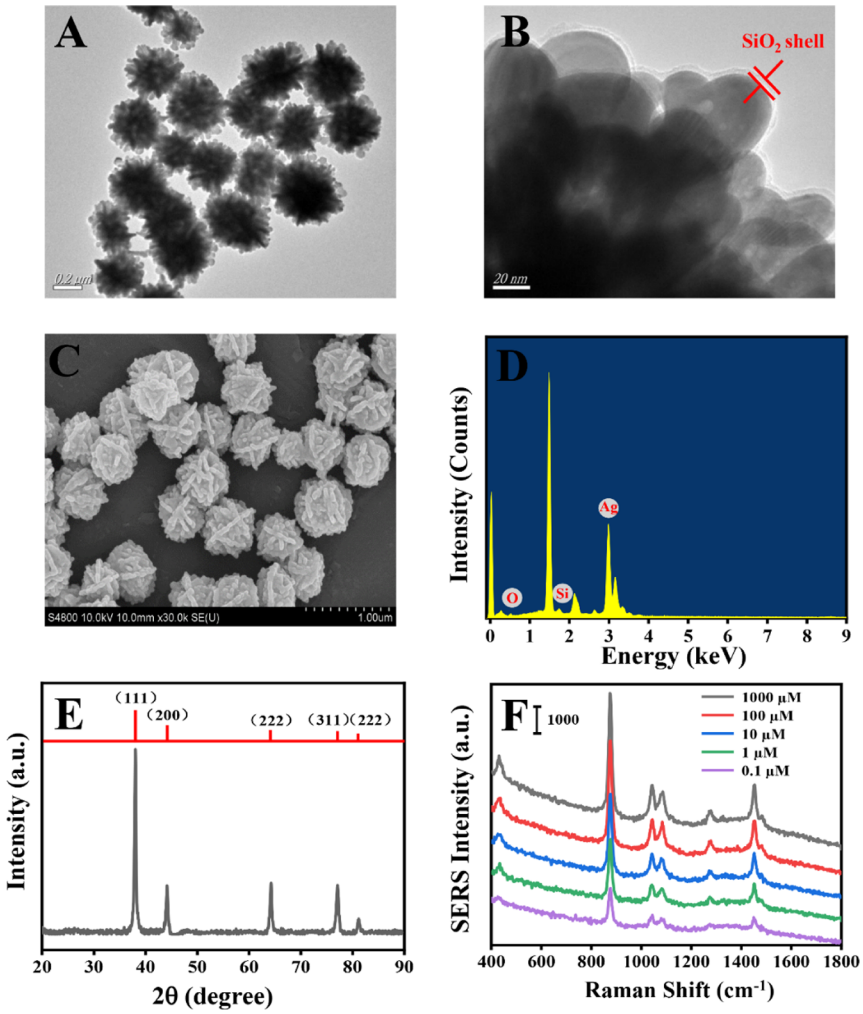

Figure 1. TEM images (A,B), FE-SEM image (C), EDS spectrum (D), and XRD plot (E) of Ag NFs@SiO_2. SERS spectrum of R6G with concentrations from 0.1 to 100 M adsorbed on Ag NFs@SiO_2 (F).

2.7. *S. aureus* Detection and Specificity of the Experiment. Initially, 500 μL of the aptamer-capped MSNs was injected into a 5 mL centrifuge tube. *S. aureus* (500 μL) solution with a known concentration was added and incubated at 37 °C for 8 min. Then, the mixture was centrifuged at 5000 rpm for 5 min at RT and the supernatant was taken for SERS detection to determine the linear range and detection limit. The measurements were carried out in triplicate.

In this experiment, *E. coli*, *V. parahaemolyticus*, *B. subtilis*, *Salmonella*, and *Pseudomonas* were selected to verify the specificity of the method. The analysis was performed under optimal conditions and the concentration of bacterial culture was around 10^5 cfu/mL.

2.8. Analysis of *S. aureus* in a Real Sample. The fish used in this experiment were bought from a local RT-Mart supermarket and transported to the laboratory in ice bags. First, 25 g of the fish meat was taken and then irradiated with an ultraviolet disinfection lamp in a super clean worktable for 30 min. The purpose of this step was to remove the interference of other foodborne pathogens. Then, different concentrations of *S. aureus* (1×10^3, 1×10^4, 1×10^5, and 1×10^6 cfu/mL) were injected into the prepared fish meat samples and incubated for 30 min. Thereafter, the spiked fish sample was transferred to a 250 mL round-bottom flask, mixed with 100 mL of sterile saline, and shaken for 3 min. Finally, the established SERS platform was used to measure the prepared samples, the results were compared with the conventional plate counting method, and the recovery rate was obtained.

3. RESULTS AND DISCUSSION

3.1. Detection Mechanism. The detection of *S. aureus* was based on the target-responsive release of the signal molecules from aptamer-gated MSNs as depicted in Scheme 1. MSNs were first synthesized by the sol−gel method, and their surfaces were modified with amino groups by APTES to produce a positive change (Scheme 1A). Then, a large number of 4-ATP molecules were loaded into the pores of MSNs by oscillating on a shaker. After that, the gates of positively charged aminated MSNs were blocked by negatively charged aptamers through electrostatic interaction (Scheme 1B). When *S. aureus* was added to the above detection system, the bacteria specifically bonded to the aptamer. This process led to the decomposition of the aminated mesoporous silica coated with aptamers. As a result, the "gate" was destroyed and 4-ATP molecules were released from the pores of MSNs for SERS detection. In this case, the obtained SERS signals were directly proportional to the *S. aureus* concentration (Scheme 1C).

3.2. Characterization of the Ag NFs@SiO_2 Substrate. Ag NFs@SiO_2 core−shell nanostructures were prepared by the hydrothermal method.[34] A seed-mediated method was first

https://doi.org/10.1021/acs.analchem.1c01280
Anal. Chem. 2021, 93, 9788−9796

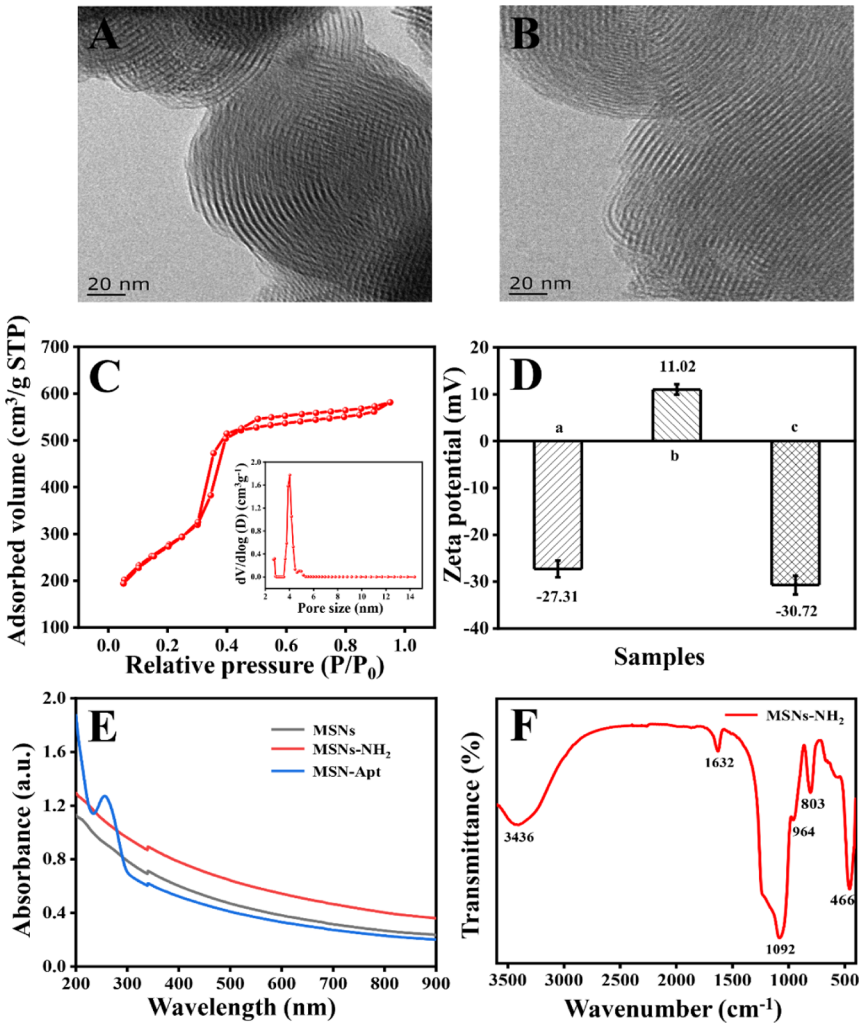

Figure 2. TEM images of MSNs at different magnifications (A,B), nitrogen adsorption−desorption isotherms (inset: pore size distribution) (C), ζ potential (D) of (a) MSNs, (b) NH_2-MSNs, and (c) aptamers−MSNs, UV−vis absorption spectra (E) of the preparation process, and FT-IR image of MSNs (F).

used to prepare Ag NFs. Then, TEOS was used as a silicon source, and the silver core was covered with a layer of the silica shell. The successful coating mechanism of SiO_2 on silver nanoparticles (Ag NPs) is that PVP has a good affinity with Ag NPs as a surfactant and can chelate with silver ions in solution. When silver ions were reduced to nano-silver particles, a large amount of PVP was adsorbed on the surface of the silver nanoparticles. The electrostatic repulsion was acquired and the silver sol was stabilized. PVP on the surface of silver nanoparticles made the surface glassy and had a good affinity with TEOS. Then, under the catalysis of ammonia, the hydrolysis and condensation reaction generated a thin SiO_2 inert shell on the surface of the silver core.

The morphologies of the Ag NFs@SiO_2 core−shell nanostructure were characterized by TEM and FE-SEM. As shown in the TEM image (Figure 1A), the synthesized Ag NFs@SiO_2 core−shell has a uniform structure with good dispersion. Similarly, the FE-SEM image (Figure 1C) exhibited that the Ag NFs@SiO_2 was spherical, with a highly rough surface, and was composed of many irregular protrusions. The average size of the Ag NFs@SiO_2 was about 300 nm and the protrusion size was about 10 nm as presented in Figure S1A,B (see the Supporting Information). Deep caves were found between these protrusions. The SiO_2 shell was successfully assembled on the surface of silver NFs. The elemental composition of Ag NFs@SiO_2 was investigated by EDS analysis. The signals of silver, silicon, and oxygen were found in the histogram of EDS (Figure 1D). Figure 1E depicts the typical XRD plot, revealing the crystal structure and phase composition of Ag NFs@SiO_2. Four diffraction peaks were noted at 2θ = 38.08, 44.28, 64.28, and 77.33° corresponding to the (111), (200), (220), and (311) crystalline planes of the face-centered-cubic structure of Ag NFs@SiO_2, respectively,[38] hence confirming that Ag NFs@SiO_2 was well crystallized. In addition, the Raman ability of Ag NFs@SiO_2 was signified by using R6G with different concentrations ranging from 0.1 to 100 μM, as presented in Figure 1F. The Raman signal intensity increased with the increasing concentration of R6G, which indicated that Ag NFs@SiO_2 can serve as highly active SERS substrates for fast SERS determination.

3.3. Characterization of Aptamer-Gated MSNs. The constructed sensor was based on the release of signal molecules (4-ATP) from aptamer-gated mesoporous silica, so the successful preparation of the aptamer-coated MSNs was particularly critical. Figure 2F shows the FT-IR spectrum of MSNs. Obvious characteristic absorption peaks were observed

https://doi.org/10.1021/acs.analchem.1c01280
Anal. Chem. 2021, 93, 9788−9796

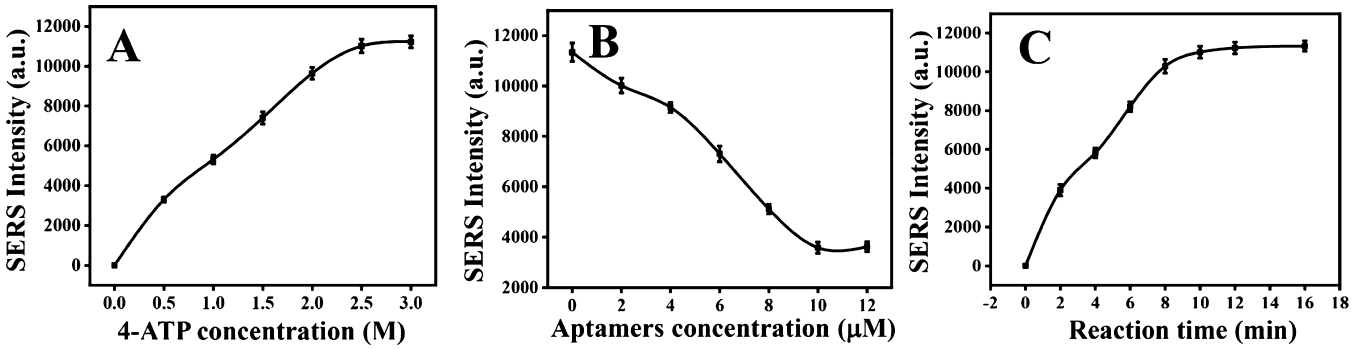

Figure 3. Dependence of the Raman signal on the (A) 4-ATP molecule concentration, (B) aptamer concentration, and (C) release time of 4-ATP molecules. The error bars were derived from the standard deviation of three measurements. Error bar = SD (n = 3).

at 3436, 1632, 1092, 964, 803, and 466 cm^{-1}. Among these, the absorption peak at 466 cm^{-1} was attributed to the bending vibration of O−Si−O, and the absorption peak at 1092 cm^{-1} was attributed to the stretching vibration of Si−O−Si. The peaks at 964 and 1632 cm^{-1} corresponded to the bending vibration of Si−OH in MSNs. The broad absorption peak at 3436 cm^{-1} was due to the O−H stretching vibration of water molecules. All the characteristic absorption peaks confirmed the successful synthesis of MSNs. Figure 2A exhibits the typical TEM image of the MSNs. The as-formed MSNs were spherical and their size was about 200 nm. In addition, the MSNs have a large number of pores, as presented in Figure 2B, which provided sufficient sites for the loading of signal molecules. As displayed in Figure 2C, the specific surface area of the MSNs was 524.3 m^2/g, which can be seen from the nitrogen adsorption−desorption isotherm (presented a typical curve). The average pore diameter was 4.2 nm (inset of Figure 2C), which was significantly larger than that of the 4-ATP molecule (equivalent to a diameter of 1.0 nm). Therefore, abundant 4-ATP molecules were loaded in the pores of MSNs. In order to corroborate whether the capped aptamers were assembled on the aminated mesoporous silica by electrostatic adsorption, we used ζ potential to monitor the MSNs gated by the aptamers after each step. The ζ potential of the MSNs was −27.31 mV recorded in column "a" of Figure 2D. When amino groups were modified on the surface of the MSNs by APTES, the aminated MSNs showed a positively charged nature and the potential was 11.02 mV (column "b" of Figure 2D). Hence, these findings illustrated that the amino groups were successfully modified on the surface of the MSNs. Because of the negatively charged aptamers, when the aptamers were assembled on the surface of the aminated MSNs by electrostatic adsorption, the aminated coated MSNs became negatively charged (−30.72 mV), as presented in Figure 2D(c). In order to further prove that the capped aptamers were assembled on the surface of the MSNs, we used UV−vis absorption spectroscopy to characterize the aptamer-functionalized MSNs (Figure 2E). The unmodified MSNs showed no characteristic UV−vis absorption peak and the adsorption curve changed slightly for aminated MSNs as compared with the MSN curve. When aptamers were assembled on the surface of the aminated MSNs, a characteristic UV−vis absorption peak appeared at 265 nm,[39] which corresponded to the DNA molecule. These results indicated that the aptamers were successfully assembled on the surface of the aminated MSNs.

3.4. Control Tests. Before optimization of the experimental conditions, we examined the stability of the aptamer-gated MSN sensing platform (details for characterization of signal molecule-loading MSNs capped with aptamers in Supporting Information, Figure S2). Two control tests were investigated using MSNs@4-ATP and MSNs@4-ATP-Apts in the absence of bacteria. The Raman signals were collected and recorded intermittently. As shown in the "black" line in Figure S2, the 4-ATP molecules were released slowly from the MSNs and reach equilibrium at about 10 min, indicating that signal molecules could not be gated in the MSNs without aptamer gating. However, in the presence of aptamers (without target bacteria), there was almost no change in the Raman signals over 16 min, demonstrating that 4-ATP molecules could be gated firmly in the pores by the adsorbed negatively charged aptamers (Figure S2, "read" line). The MSNs@4-ATP-Apts were very stable with nearly zero leakage during storage. For comparison, the trigger release of signal molecules was monitored by adding 500 μL of *S. aureus* solution to the MSNs@4-ATP-Apts system. The signals of Raman were raised within 8 min and then no longer changed with time ("blue" line in Figure S2), revealing a rapid decomposition of aptamers by bacteria at RT. Longer incubation times did not contribute to the signals, and hence, in this assay, all Raman signals were recorded after a reaction of 8 min. In addition, to verify the coating system of aptamer-gated mesoporous silica. After the aptamers were assembled on MSNs and loaded with signal molecules, the Raman signals of 4-ATP and the UV−vis absorption spectra of the aptamers in the supernatant were measured (see Supporting Information, Figure S3A,B). After 3 times of centrifugal cleaning, the UV−vis absorption of aptamers and Raman signal of 4-ATP in the supernatant decreased continuously and reached an unobvious level for the third time.

3.5. Optimization of Experimental Conditions. In this work, the measured Raman signal intensity mainly came from the loaded 4-ATP molecules in the pores of aminated MSNs. Therefore, the sensitivity of the aptamer-coated MSN-based SERS biosensor was dependent on the amount of 4-ATP molecules. Herein, the effects of different concentrations of 4-ATP molecules were first explored. Initially, 500 μL of the aptamer-capped MSNs with different concentrations of 4-ATP was added into a 5 mL centrifuge tube. *S. aureus* (500 μL) solution was injected into the mixture and incubated at 37 °C for 8 min. Subsequently, the mixture was centrifuged at 5000 rpm for 5 min at RT and the supernatant was taken for SERS detection. As exhibited in Figure 3A, the Raman intensity increased with the increment of 4-ATP concentration and tended to be horizontal after 2.5 M 4-ATP molecules. This

https://doi.org/10.1021/acs.analchem.1c01280
Anal. Chem. 2021, 93, 9788−9796

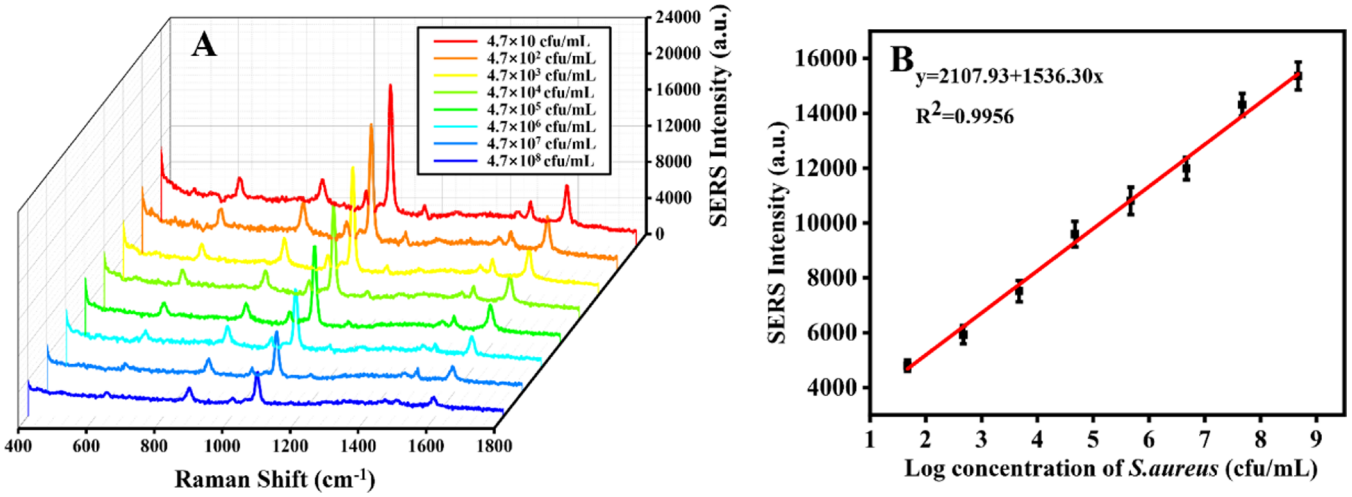

Figure 4. SERS spectra of varying concentrations of *S. aureus* (A) and the correlation between Raman intensity and concentration of *S. aureus* (B).

Table 1. Comparison of the Results Acquired via This Method with the Conventional Plate Counting Method on the Spike Recovery of Fish Samples[a]

samples	spiked (cfu/mL)	plate counting method ±SD (cfu/mL)	this method ±SD (cfu/mL)	RSD %	recovery %	*P*
1	1×10^3	$(0.901 \pm 0.03) \times 10^3$	$(0.913 \pm 0.04) \times 10^3$	4.38	91.3	$P = 0.315$
2	1×10^4	$(0.952 \pm 0.05) \times 10^4$	$(1.02 \pm 0.05) \times 10^4$	4.90	102	
3	1×10^5	$(1.07 \pm 0.03) \times 10^5$	$(1.09 \pm 0.04) \times 10^5$	3.67	109	
4	1×10^6	$(0.974 \pm 0.04) \times 10^6$	$(0.943 \pm 0.03) \times 10^6$	3.18	94.3	

[a]SD: standard deviation, $n = 3$. $P > 0.05$ indicates no significant difference.

may be because a high concentration of 4-ATP changed the viscosity of the reaction solution. Therefore, 2.5 M 4-ATP was selected as the optimal concentration for the biosensor.

In addition, the concentration of aptamers is another crucial parameter to influence the detection sensitivity. Aptamers with different concentrations were added into 500 μL of 2.5 M signal molecule solution (containing 5 mg of MSNs) and then centrifuged and washed with water to obtain MSNs@4-ATP-Apts. When 500 μL of *S. aureus* liquid was added, the supernatant was centrifuged and the Raman signal was detected. The SERS intensity decreased with the increase of aptamer concentration up to 10 μM, and after 10 μM, no obvious change was observed. Thus, 10 μM was regarded as the optimal aptamer concentration, as shown in Figure 3B.

The reaction time of *S. aureus* and aptamers on the surface of aminated MSNs directly affected the SERS signal of the established method. The Raman intensity increased with the increasing reaction time and reached equilibrium after 8 min, as depicted in Figure 3C, hence indicating that the reaction between bacteria and aptamers accompanied the 4-ATP release and a dynamic balance was reached.

3.6. Linear Range and Detection Limit. Under optimal conditions, the constructed SERS sensor platform was employed to quantify different concentrations of *S. aureus* based on target-responsive controlled release of 4-ATP molecules from aptamer-gated MSNs. The detection was carried out using a Raman spectrometer after *S. aureus* solution was added to the aptamer-coated MSNs for 8 min at RT. As depicted in Figure 4A, the Raman signal intensity increased with the increasing concentration of the bacteria. A linear relation between Raman intensity and *S. aureus* concentration was acquired in the range from 4.7×10 to 4.7×10^8 cfu/mL. The linear regression equation was $y = 2107.93 + 1536.30x$, $R^2 = 0.9956$ (Figure 4B). The detection limit was calculated by the formula $LOD = 3S/M$, where S is the standard deviation of the blank sample (without *S. aureus*) and M is the slope of the standard curve. The limit of detection (LOD) was 17 cfu/mL, according to the rule of 3 times the standard deviation of the blank signal. In addition, compared with other previously reported methods for the determination of *S. aureus*, the detection limit of this method is lower or equivalent (see Supporting Information Table S1).

3.7. Result of a Specificity Experiment. To confirm the selectivity and specificity of the aptamer-gated MSN biosensor for *S. aureus* detection, the Raman signals were recorded in the presence of other foodborne pathogens including *E. coli*, *V. parahaemolyticus*, *B. subtilis*, *Salmonella*, *Pseudomonas*, and *L. monocytogenes*. In order to get the best experimental results, a bacterial concentration of 10^5 cfu/mL was selected. The results of the specificity analysis are shown in Figure S4 (details for the results of specificity experiment are provided in the Supporting Information). Compared with *E. coli*, *V. parahaemolyticus*, *B. subtilis*, *Salmonella*, *Pseudomonas*, and *L. monocytogenes*, *S. aureus* exhibited a dramatically strong Raman signal at 1071 cm^{-1}, indicating that this method has good specificity and could be specifically applied for the detection of *S. aureus*.

3.8. Application Analysis in Fish Samples. The platform based on aptamer-gated MSNs for *S. aureus* detection was used for the blank spike recovery test of fish samples. *S. aureus* with different concentrations from 1×10^3 to 1×10^6 cfu/mL was detected by the established method and conventional plate counting method, respectively. The fish samples of each concentration were repeated three times, and then the obtained results were compared to calculate the recovery rate. The results showed that the method has good

https://doi.org/10.1021/acs.analchem.1c01280
Anal. Chem. 2021, 93, 9788−9796

accuracy for the quantitative detection of *S. aureus*, and the recoveries were between 91.3 and 109%, which could be used for the detection of *S. aureus* in actual samples, as shown in Table 1.

4. CONCLUSIONS

In this study, a simple and sensitive sensing platform for the quantitative determination of *S. aureus* was established by using target-responsive release of signal molecules (4-ATP molecules) from aptamer-gated MSNs. The capped aptamers served as the "gate" for the blocking and releasing of the 4-ATP molecules from the pores of MSNs. Under optimal experimental conditions, a linear relation between Raman intensity and *S. aureus* concentration was achieved in the range from 4.7×10 to 4.7×10^8 cfu/mL. The linear regression equation was $y = 2107.93 + 1536.30x$, $R^2 = 0.9956$, and the LOD was 17 cfu/mL. In addition, no significant difference between the spiked recovery rate test of fish samples and the plate counting method was observed and the spiked recovery rate was 91.3−109%, indicating that this method can be used for the detection of actual samples. Moreover, compared with other detection methods, the proposed SERS-based sensing platform is low-cost, rapid, and sensitive, which is more reliable for the detection of foodborne pathogens in a food matrix. However, a simultaneous detection system for other types of pathogenic bacteria or multi-target bacteria needs to be further investigated based on this study.

■ ASSOCIATED CONTENT

Supporting Information

The Supporting Information is available free of charge at https://pubs.acs.org/doi/10.1021/acs.analchem.1c01280.

Characterization of the Ag NF silica core−shell structure (Ag NFs@SiO_2), characterization of signal molecule-loading MSNs capped with aptamers, control tests and the results of the specificity experiment, and data about the comparison of this method with other reported detection methods (PDF)

■ AUTHOR INFORMATION

Corresponding Authors

Qin Ouyang − *School of Food and Biological Engineering, Jiangsu University, Zhenjiang 212013, P. R. China*; Email: oyqyf@ujs.edu.cn

Quansheng Chen − *School of Food and Biological Engineering, Jiangsu University, Zhenjiang 212013, P. R. China*; orcid.org/0000-0003-2498-3278; Phone: +86-511-88790318; Email: qschen@ujs.edu.cn; Fax: +86-511-88780201

Authors

Afang Zhu − *School of Food and Biological Engineering, Jiangsu University, Zhenjiang 212013, P. R. China*

Tianhui Jiao − *School of Food and Biological Engineering, Jiangsu University, Zhenjiang 212013, P. R. China*

Shujat Ali − *College of Electrical and Electronic Engineering, Wenzhou University, Wenzhou 325035, P. R. China*

Yi Xu − *School of Food and Biological Engineering, Jiangsu University, Zhenjiang 212013, P. R. China*

Complete contact information is available at: https://pubs.acs.org/10.1021/acs.analchem.1c01280

Author Contributions

A.Z. and T.J. contributed equally to this work and should be considered co-first authors. A.Z. handled methodology, investigation, and writing the original draft. T.J. handled visualization, data curation, and writing—review and editing. S.A. handled software, formal analysis, investigation, and writing—review and editing. Y.X. handled conceptualization and investigation. Q.O. handled validation and data curation. Q.C. handled conceptualization and supervision.

Notes

The authors declare no competing financial interest.

■ ACKNOWLEDGMENTS

This work has been financially supported by the National Key Research and Development Program of China (2017YFC1600801), the Natural Science Foundation of Jiangsu Province (BK20190100), and the Project of Faculty of Agricultural Equipment of Jiangsu University.

■ REFERENCES

(1) Cook-Mills, J. M.; Kaplan, M. H.; Turner, M. J.; Kloepfer, K. M.; Kumar, R. *J. Allergy Clin. Immunol.* **2019**, *144*, 404−406.

(2) Wakabayashi, Y.; Umeda, K.; Yonogi, S.; Nakamura, H.; Yamamoto, K.; Kumeda, Y.; Kawatsu, K. *Int. J. Food Microbiol.* **2018**, *265*, 23−29.

(3) Oh, W. T.; Jun, J. W.; Giri, S. S.; Yun, S.; Kim, H. J.; Kim, S. G.; Kim, S. W.; Han, S. J.; Kwon, J.; Park, S. C. *Microorganisms* **2019**, *7*, 330.

(4) Yu, Z.; Peruzy, M. F.; Dumolin, C.; Joossens, M.; Houf, K. *Food Microbiol.* **2019**, *82*, 53−61.

(5) Huang, Q.; Zhao, B.; Bold, S.-E.; Bu, T.; Yan, L.; Dou, L.; Yang, Q.; Wang, J.; Zhang, D. *Sens. Actuators, B* **2019**, *288*, 210−216.

(6) Wu, D.; Shi, B.; Li, B.; Wu, W. *IEEE Access* **2020**, *8*, 99598−99604.

(7) Ma, X.; Ding, W.; Wang, C.; Wu, H.; Tian, X.; Lyu, M.; Wang, S. *Sens. Actuators, B* **2021**, *331*, 129422.

(8) Chen, J.; Xu, Y.; Yan, H.; Zhu, Y.; Wang, L.; Zhang, Y.; Lu, Y.; Xing, W. *Lab Chip* **2018**, *18*, 2441−2452.

(9) He, S.; Hong, X.; Zhang, M.; Wu, L.; Yan, X. *Anal. Chem.* **2020**, *92*, 2393−2400.

(10) Schlücker, S. *Angew. Chem., Int. Ed.* **2014**, *53*, 4756−4795.

(11) Kutsanedzie, F. Y. H.; Agyekum, A. A.; Annavaram, V.; Chen, Q. *Food Chem.* **2020**, *315*, 126231.

(12) Li, Y.-S.; Church, J. S. *J. Food Drug Anal.* **2014**, *22*, 29−48.

(13) Wang, J.; Ahmad, W.; Mehedi Hassan, M.; Zareef, M.; Viswadevarayalu, A.; Arslan, M.; Li, H.; Chen, Q. *Food Chem.* **2020**, *323*, 126812.

(14) Pérez-Jiménez, A. I.; Lyu, D.; Lu, Z.; Liu, G.; Ren, B. *Chem. Sci.* **2020**, *11*, 4563−4577.

(15) Guo, J.; Zeng, F.; Guo, J.; Ma, X. *J. Mater. Sci. Technol.* **2020**, *37*, 96−103.

(16) Ai, Y.-j.; Liang, P.; Wu, Y.-x.; Dong, Q.-m.; Li, J.-b.; Bai, Y.; Xu, B.-J.; Yu, Z.; Ni, D. *Food Chem.* **2018**, *241*, 427−433.

(17) Xu, J.; Li, X.; Wang, Y.; Hua, T.; Guo, R.; Miao, D.; Jiang, S. *Cellulose* **2019**, *27*, 941−954.

(18) Ong, T. T. X.; Blanch, E. W.; Jones, O. A. H. *Sci. Total Environ.* **2020**, *720*, 137601.

(19) Wen, S.; Ma, X.; Liu, H.; Chen, G.; Wang, H.; Deng, G.; Zhang, Y.; Song, W.; Zhao, B.; Ozaki, Y. *Anal. Chem.* **2020**, *92*, 11763−11770.

(20) Xu, Y.; Kutsanedzie, F. Y. H.; Hassan, M.; Zhu, J.; Ahmad, W.; Li, H.; Chen, Q. *Food Chem.* **2020**, *315*, 126300.

(21) Wang, J.; Hassan, M. M.; Ahmad, W.; Jiao, T.; Xu, Y.; Li, H.; Ouyang, Q.; Guo, Z.; Chen, Q. *Sens. Actuators, B* **2019**, *285*, 302−309.

(22) Dai, X.; Song, Z.-L.; Song, W.; Zhang, J.; Fan, G.-C.; Wang, W.; Luo, X. *Anal. Chem.* **2020**, *92*, 11469−11475.

(23) Xu, Y.; Kutsanedzie, F. Y. H.; Hassan, M. M.; Zhu, J.; Li, H.; Chen, Q. *Sens. Actuators, B* **2020**, *324*, 128718.
(24) Jiao, T.; Mehedi Hassan, M.; Zhu, J.; Ali, S.; Ahmad, W.; Wang, J.; Lv, C.; Chen, Q.; Li, H. *Food Chem.* **2021**, *337*, 127652.
(25) Li, H.; Chen, Q.; Mehedi Hassan, M.; Chen, X.; Ouyang, Q.; Guo, Z.; Zhao, J. *Biosens. Bioelectron.* **2017**, *92*, 192−199.
(26) Li, H.; Liu, S.; Hassan, M. M.; Ali, S.; Ouyang, Q.; Chen, Q.; Wu, X.; Xu, Z. *Spectrochim. Acta, Part A* **2019**, *223*, 117281.
(27) Sun, Y.; Zhang, H.; Wang, Y.; Wang, Y. *J. Controlled Release* **2017**, *259*, e45−e46.
(28) Tang, D.; Liu, B.; Niessner, R.; Li, P.; Knopp, D. *Anal. Chem.* **2013**, *85*, 10589−10596.
(29) Yue, Q.; Sun, J.; Kang, Y.; Deng, Y. *Angew. Chem., Int. Ed.* **2020**, *59*, 15804−15817.
(30) Tan, Q.; Zhang, R.; Kong, R.; Kong, W.; Zhao, W.; Qu, F. *Microchim. Acta* **2018**, *185*, 44.
(31) Zhang, B.; Liu, B.; Liao, J.; Chen, G.; Tang, D. *Anal. Chem.* **2013**, *85*, 9245−9252.
(32) Yang, M.; Liu, G.; Mehedi, H. M.; Ouyang, Q.; Chen, Q. *Anal. Chim. Acta* **2017**, *986*, 122−130.
(33) Li, J.; Jiang, H.; Rao, X.; Liu, Z.; Zhu, H.; Xu, Y. *Anal. Chem.* **2019**, *91*, 1494−1500.
(34) Zheng, H.; Ni, D.; Yu, Z.; Liang, P.; Chen, H. *Sens. Actuators, B* **2016**, *231*, 423−430.
(35) Wei, A.; Yao, Y.; Wang, T.; Shen, L.; Jia, L.; Chen, S. *Mater. Lett.* **2018**, *230*, 236−240.
(36) Qian, R.; Ding, L.; Ju, H. *J. Am. Chem. Soc.* **2013**, *135*, 13282−13285.
(37) Wang, Y.; Lu, M.; Zhu, J.; Tian, S. *J. Mater. Chem. B* **2014**, *2*, 5847−5853.
(38) Liang, Y.; Chen, Z.; Yao, W.; Wang, P.; Yu, S.; Wang, X. *Langmuir* **2017**, *33*, 7606−7614.
(39) Gopinath, S. C. B.; Hashim, U.; Uda, M. N. A. *AIP Conf. Proc.* **2017**, *1808*, 020018.

https://doi.org/10.1021/acs.analchem.1c01280
Anal. Chem. 2021, 93, 9788−9796